Electronic Absorption and Fluorescence Properties of 2,5-Diarylidene-Cyclopentanones

Robert E. Connors* and Mine G. Ucak-Astarlioglu

Department of Chemistry and Biochemistry, Worcester Polytechnic Institute, Worcester, Massachusetts 01609

Received: August 27, 2002; In Final Form: May 21, 2003

Spectroscopic properties for a series of 2,5-diarylidene-cyclopentanones are reported. Electronic absorption and fluorescence spectra have been measured for the all-*E* configurations of 2,5-dibenzylidene-cyclopentanone (**1**), 2,5-bis-(3-phenyl-allylidene)-cyclopentanone (**2**), and 2,5-bis-(5-phenyl-penta-2,4-dienylidene)-cyclopentanone (**3**). The absorption spectra have been assigned with the aid of INDO/S calculations. Molecular structures used for the INDO/S calculations were computed with the PM3 Hamiltonian. Agreement between absorption spectra obtained in cyclohexane at room temperature and the theoretical predictions is good. For **1**, **2**, and **3** the general features of the spectra are similar. The transition to S_1 (weak) is assigned as $n \rightarrow \pi^*$ ($A_2 \leftarrow A_1$), to S_2 (strong) as $\pi \rightarrow \pi^*$ ($B_2 \leftarrow A_1$), and to S_3 (moderate) as $\pi \rightarrow \pi^*$ ($A_1 \leftarrow A_1$). The energy gap between S_1 and S_2 is seen to decrease as the length of the polyene chain increases in going from **1** to **3**. Fluorescence is not observed for **1** in any of the solvents studied (protic and aprotic). Fluorescence is observed for **2** in protic solvents only. For **3**, fluorescence is observed in a number of protic and aprotic solvents. Solvents which are able to induce fluorescence are believed to do so by inverting the order of $^1(n\pi^*)$ and $^1(\pi\pi^*)$ states. The influence of hydrogen bonding on the excitation spectra of **2** and **3** is discussed. Solvent-induced shifts in the absorption and fluorescence spectra of **3** in combination with the PM3 calculated ground-state dipole moment (2.8 D) are used to determine the excited-state dipole moment of **3** (6.4 D/protic solvents; 6.6 D/aprotic solvents). Fluorescence quantum yields in different solvents for **3** vary as the fluorescence maxima shift in these solvents, going through a maximum in the mid-frequency range. The variation in quantum yields with different solvents is primarily attributed to changes in the nonradiative rate of decay from S_1. Excitation, polarized excitation, and fluorescence spectra have been measured for **2** and **3** at 77 K in ethanol/methanol glass. Vibronic features not observed in the broad spectra obtained in alcohols at room temperature become clearly resolved at 77 K. Evidence is provided that indicates that **2** and **3** undergo excited-state proton-transfer reactions in acetic acid at room temperature.

Introduction

Substituted and unsubstituted 2,5-diarylidene-cyclopentanones (Figure 1), a class of diarylpolyene ketones, have received recent attention for their potential applications in a variety of areas. These include use as photosensitizers and photopolymer imagers,[1] solvent polarity probes,[2] fluoroionophores,[3] and nonlinear optical materials.[4] In addition, interesting photodimerization reactions that have implications for crystal engineering have been reported for crystalline 2,5-dibenzylidene-cyclopentanone (R = H, $n = 1$, Figure 1).[5] Despite the considerable interest in applications related to their photoexcited-state properties, little has been reported describing the electronic structure and spectroscopy of these molecules.[6] We have begun an investigation of the electronic structure, as well as the absorption and luminescence properties, of molecules represented in Figure 1. The focus of this initial report is on the all-*E* configurations of the unsubstituted parent compounds (R = H) with $n = 1$, 2, and 3: 2,5-dibenzylidene-cyclopentanone (**1**), 2,5-bis-(3-phenyl-allylidene)-cyclopentanone (**2**), and 2,5-bis-(5-phenyl-penta-2,4-dienylidene)-cyclopentanone (**3**) (see Figure 2). The combination of aryl, carbonyl, and polyene chromophores presents an interesting challenge for molecular orbital methods to provide insight as to the nature of the spectral transitions. Any discussion of the electronic structure and spectroscopy of molecules containing polyene chains brings to mind the considerable body of work regarding the relative location of the symmetry forbidden 2^1A_g state (under C_{2h} symmetry) and the strongly

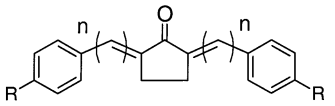

Figure 1. Structure of 2,5-diarylidene-cyclopentanones.

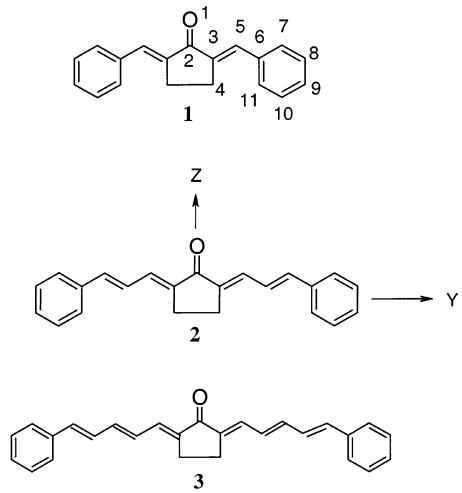

Figure 2. Molecular structures of **1**, **2**, and **3**.

* Corresponding author. Phone: (508) 831-5394. Fax: (508) 831-5933. E-mail rconnors@wpi.edu.

10.1021/jp0219597 CCC: $25.00
Published on Web 08/30/2003

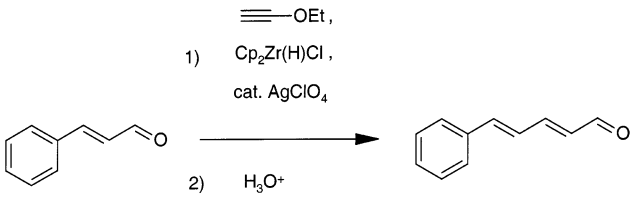

Figure 3. Reaction scheme for the synthesis of 5-phenyl-penta-2,4-dienal.

allowed 1^1B_u state.[7] Comparison with previous work on polyene aldehydes and ketones will be given where pertinent throughout the paper.

Experimental Section

Compounds **1** and **2** were synthesized by the $RuCl_3$ catalyzed aldol cross condensation of cyclopentanone with benzaldehyde and cinnamaldehyde, respectively.[8] Compound **3** was prepared by the base-catalyzed condensation of cyclopentanone with 5-phenyl-penta-2,4-dienal. The dienal was synthesized by two carbon homologation of cinnamaldehyde using $AgClO_4$ catalyzed addition of the zirconocene complex derived from the hydrozirconation of 1-ethoxyethyne (Aldrich) with bis(cyclopentadienyl)zirconium chloride hydride (Strem) followed by acidic hydrolysis, as shown in Figure 3.[9] All final products were purified by recrystallization or column chromatography, and their purity was confirmed by HPLC.

Absorption spectra were measured with a Schimadzu UV2100U spectrometer (2-nm band-pass). Fluorescence spectra were obtained with a Perkin-Elmer LS 50B luminescence spectrometer equipped with a R928 phototube. Fluorescence quantum yields (ϕ_f), corrected for differences in refractive indices, were determined by comparing corrected integrated fluorescence spectra with that of coumarin 481 (Exciton), also known as coumarin 35, in acetonitrile, with ϕ_f taken as 0.11.[10] Absorbance at the wavelength of excitation was kept low (<0.08). Degassing of solutions had no measurable affect on the ϕ_f values. Fluorescence spectra used to determine ϕ_f were corrected using correction factors that were obtained by measuring the spectra of compounds with known emission spectra.[11] Other fluorescence spectra were uncorrected. All excitation spectra were corrected for instrumental response. The band-pass was 5 nm for both the excitation and emission monochromators. Low-temperature fluorescence measurements were made with either a quartz optical dewar (77 K) or an Air Products Displex 202 closed-cycle refrigeration system (10 K). Attempts to observe phosphorescence out to 850 nm for **1**, **2**, and **3** in various solvents at 77 K were unsuccessful.

Because there is limited X-ray crystallographic data available for the structures discussed here, computed geometries were used as input for our spectral calculations. Fully optimized structures, as confirmed by finding all positive force constants for the computed normal modes of vibration, were obtained with the PM3 Hamiltonian[12] using the MOPAC 2000 program. Spectral properties were calculated for the optimized structures using the INDO/S Hamiltonian[13] with configuration interaction as implemented in the MOS-F (V.4.2) program. Complete sets of singly excited configurations (SCI) were employed in the calculations for **1** and **2**; 25 000 SCI configurations were employed for **3**. The calculations were also carried out using 49 SCI and 96 doubly excited configurations (DCI). It was found that slightly better agreement between the calculated and experimental band positions was obtained with the SCI calculations.

TABLE 1: Calculated and Experimental Geometry of 1

	bond lengths (Å)		bond order
	PM3	expt.[a]	PM3
O_1-C_2	1.216	1.210	1.88
C_2-C_3	1.491	1.474	0.95
C_3-C_4	1.493	1.493	0.99
C_3-C_5	1.340	1.341	1.84
C_5-C_6	1.460	1.461	1.03
C_6-C_7	1.400	1.389	1.38
C_7-C_8	1.389	1.387	1.44
C_8-C_9	1.391	1.356	1.41
C_9-C_{10}	1.390	1.373	1.42
$C_{10}-C_{11}$	1.390	1.385	1.43
$C_{11}-C_6$	1.397	1.377	1.39

	bond angles (°)	
	PM3	expt.[a]
$C_1-C_2-C_3$	126.1	125.6
$C_2-C_3-C_4$	109.0	108.8
$C_4-C_3-C_5$	127.8	130.6
$C_3-C_5-C_6$	126.6	131.1
$C_5-C_6-C_7$	118.3	118.4
$C_6-C_7-C_8$	120.2	121.4
$C_7-C_8-C_9$	120.2	120.1
$C_8-C_9-C_{10}$	119.9	119.8
$C_9-C_{10}-C_{11}$	120.2	120.1
$C_{10}-C_{11}-C_6$	120.2	121.4
$C_{11}-C_6-C_7$	119.2	117.2

	dihedral angle (°)	
	PM3	expt.[a]
$C_3-C_5-C_6-C_{11}$	35.5	3.0

[a] From ref 5c.

Results and Discussion

PM3 Optimized Geometries. Initial structures for geometry optimization were drawn with all carbon and oxygen atoms in, or nearly in, the same plane. After minimization it was found that **1** had adopted a structure with C_s symmetry and **2** and **3** had found minima of C_{2v} symmetry. The major difference between the C_s and C_{2v} forms is the degree to which the phenyl rings are rotated out-of-plane. PM3 predicts that the phenyl groups of **1** are rotated 35° out-of-plane relative to the cyclopentanone ring whereas **2** and **3** have nearly planar structures. A crystallographic structure determination has been reported for **1**.[5c] The results of this study along with the PM3 calculated results are presented in Table 1. In general the agreement is good except for the out-of-plane rotation angle of the phenyl group which is 3.0° in the crystal phase. However, crystal packing forces may be responsible for the deviation of this experimental structural parameter from the calculated value.[14] Most of the computed structural parameters for **2** and **3** are similar to those of **1**. All three compounds are predicted to have a carbonyl group bond length of 1.216 Å. The single bond connected to the phenyl group is predicted to have a bond length of 1.460 Å for **1** and 1.458 Å for both **2** and **3**. The other exocyclic C−C single bond lengths fall in the range 1.448−1.449 Å for **2** and **3**. The exocyclic double bond lengths fall in the relatively narrow range of 1.340−1.344 Å for **1**, **2**, and **3**. Rotation of the phenyl rings out of the plane of the cyclopentanone ring is predicted by PM3 to be less than 0.5° for **2** and **3**.

Absorption Spectra and INDO/S Calculations. The room-temperature absorption spectra of **1**, **2**, and **3** in cyclohexane are shown in Figures 4−6 along with the results of INDO/S-CIS calculations. The spectra are similar in their gross appear-

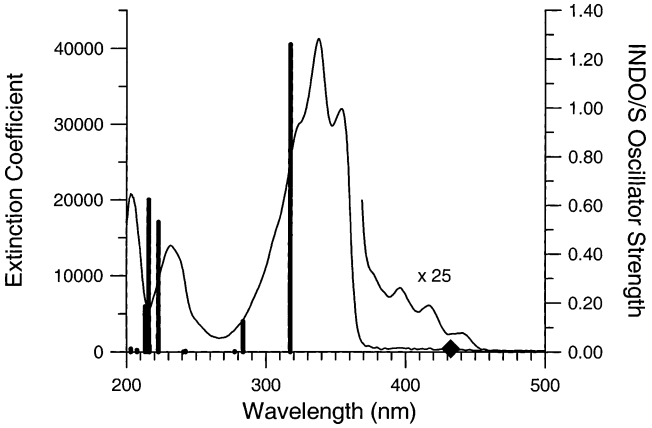

Figure 4. Room-temperature absorption spectra of **1** in cyclohexane and INDO/S-CIS calculated results. The diamond on the wavelength axis indicates the computed location of the forbidden $^1A_2 \leftarrow {}^1A_1$ transition.

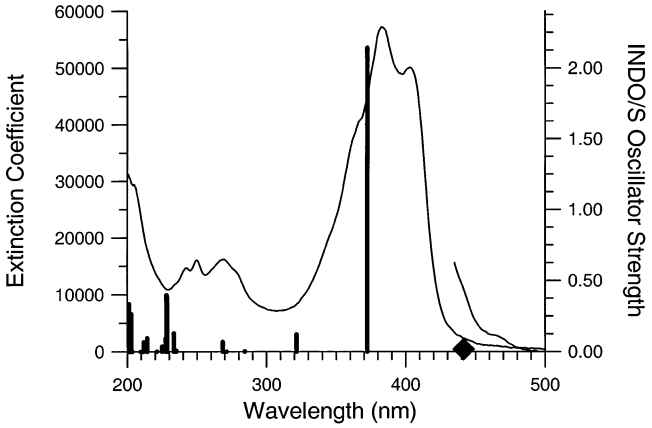

Figure 5. Room-temperature absorption spectra of **2** in cyclohexane and INDO/S-CIS calculated results. The diamond on the wavelength axis indicates the computed location of the forbidden $^1A_2 \leftarrow {}^1A_1$ transition.

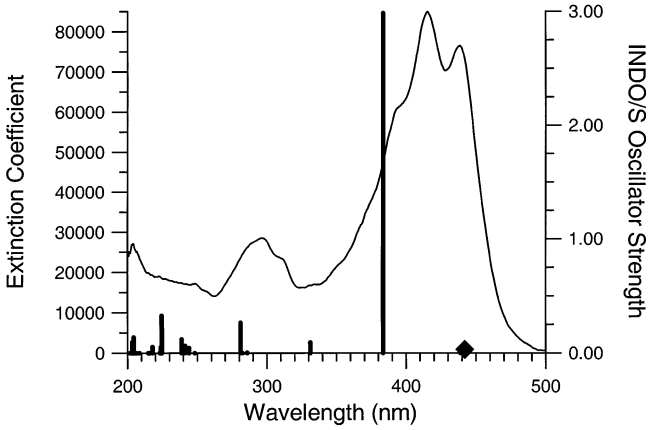

Figure 6. Room-temperature absorption spectra of **3** in cyclohexane and INDO/S-CIS calculated results. The diamond on the wavelength axis indicates the computed location of the forbidden $^1A_2 \leftarrow {}^1A_1$ transition.

ance. The dominant feature is a strong structured band found between 270 and 370 nm for **1** that moves to longer wavelength and becomes more intense as the polyene chain length increases: 320−420 nm for **2**, and 360−470 nm for **3**. The low-resolution spacing between the apparent 0−0 and 0−1 vibronic bands of the strong transition falls in the range 1300−1440 cm^{-1} for these compounds. Oscillator strengths (*f*), uncorrected for solvent index of refraction, have been determined by measuring the area under the strong transition. On the long wavelength side of the strong transition for **1** a series of weak bands with an average spacing of 1280 cm^{-1} is observed between 370 and 460 nm. This band system merges into the long wavelength shoulder of the strong structured transition. For **2**, less resolved weak shoulders are observed between 430 and 490 nm on the long wavelength side of the strong band system. These weak long wavelength bands disappear for **1** and **2** when methanol is used as the solvent. Although no clearly resolved bands are observed for **3** on the long wavelength side of the strong transition. It will be argued later that there is a separate unresolved transition in this region that is masked by the tail of the intense absorption. Turning to the short wavelength side of the strong transition, moderate absorption is observed to fall between 215 and 260 nm for **1**, 230 and 290 nm for **2**, and 260 and 320 nm for **3**. Absorption is seen to rise again near the 200-nm cutoff for all three compounds.

INDO/S calculations provide insight as to the nature of the long wavelength electronic transitions. Specific comments will be restricted to excitations terminating at the lowest three excited singlet states, S_1-S_3. For **1**, **2**, and **3**, S_1 is computed to be a symmetry forbidden $A_2 \leftarrow A_1$ transition (under C_{2v} point group) of the $n \rightarrow \pi^*$ type, arising primarily from the orbital excitation $b_2(n) \rightarrow b_1(\pi^*)$, where $b_1(\pi^*)$ is the LUMO and $b_2(n)$ is HOMO-6 for **3** and HOMO-4 for **1** and **2**. The weak bands observed between 370 and 460 nm for **1** and between 430 and 490 nm for **2** are assigned to this transition. There, position, intensity, and disappearance in alcohol solvent are entirely consistent with $n \rightarrow \pi^*$ behavior.[15] Although not separately resolved from the neighboring strong transition, it is believed that S_1 is also $n \rightarrow \pi^*$ ($A_2 \leftarrow A_1$) for **3** in cyclohexane. Fluorescence data presented below support this assignment. According to the INDO/S calculations, S_2 is a strong, *y*-polarized $B_2 \leftarrow A_1$ transition corresponding primarily to the HOMO $\rightarrow$ LUMO, $a_2(\pi) \rightarrow b_1(\pi^*)$ configuration. Clearly, the strong structured transition that dominates the spectra of the three compounds can be assigned with confidence to this excitation. This transition correlates with the $1^1B_u \leftarrow 1^1A_g$ transition of an idealized polyene under the C_{2h} point group. The transition to S_3 is computed by INDO/S−SCI to be a weak, *z*-polarized $A_1 \leftarrow A_1$ excitation with primary configurations HOMO-1 $\rightarrow$ LUMO, $a_2(\pi) \rightarrow a_2(\pi^*)$ and HOMO $\rightarrow$ LUMO + 1, $b_1(\pi) \rightarrow b_1(\pi^*)$. When the calculation is repeated to include doubly excited configurations additional important configurations are found to be HOMO-1, HOMO $\rightarrow$ LUMO, LUMO + 1, and HOMO, HOMO $\rightarrow$ LUMO, LUMO. It appears that this state correlates with the forbidden idealized polyene $2^1A_g \leftarrow 1^1A_g$ transition which is known to be S_1 for longer polyene molecules. It would be difficult to observe this relatively weak transition directly in absorption because it is predicted to overlap the short wavelength tail of the much stronger $B_2 \leftarrow A_1$ transition for **1**, **2**, and **3**. However, results from polarized fluorescence excitation spectra (see below) are consistent with the INDO/S prediction that there is a weak transition underlying the tail of the strong band system. Table 2 summarizes experimental and computed results for electronic transitions between the ground state and the excited states S_1-S_3 of **1**, **2**, and **3**.

Fluorescence Properties. In examining the fluorescence properties of these compounds it is found that each behaves differently with respect to changes in solvent polarity and hydrogen bonding strength. No fluorescence has been observed for **1** in any of the solvents studied (nonpolar, polar aprotic, or protic solvents). Fluorescence is observed for **2** in alcohols but

TABLE 2: Absorption Spectral Data for 1, 2, and 3 in Cyclohexane at Room Temperature and INDO/S Calculated Results

	1	**2**	**3**
	S_1 (A_2)		
λ (nm), exp	370−460	430−490	−
E (10^3 cm^{-1}), exp	27.0−21.7	23.3−20.4	
ϵ (M^{-1} cm^{-1})	$\sim 10^2$	$\sim 10^2$	−
λ_{max} (nm), calc	432	439	439
E (10^3 cm^{-1}), calc	23.1	22.8	22.8
f, calc	0.00	0.00	0.00
	S_2 (B_2)		
λ_{max} (nm), exp	337	382	415
E ($10^3 cm^{-1}$), exp	29.7	26.2	24.1
ϵ_{max} (M^{-1} cm^{-1})	41.2×10^3	57.2×10^3	84.9×10^3
f, exp	0.76	1.05	1.64
λ_{max} (nm), calc	317	372	383
E (10^3 cm^{-1}), calc	31.5	26.9	26.1
f, calc	1.26	2.14	2.98
	S_3 (A_1)		
λ_{max} (nm), calc	284	321	331
E (10^3 cm^{-1}), calc	35.2	31.2	30.2
f, calc	0.12	0.12	0.09

not in nonpolar or aprotic polar solvents. For **3**, fluorescence is observed in a variety of solvents including polar protic and aprotic solvents and some aprotic nonpolar solvents. However, no fluorescence has been observed for **3** in alkane solvents.

In situations where fluorescence has not been observed for **1**, **2**, or **3**, it is believed that S_1 is $n\pi^*$ and S_2 is $\pi\pi^*$. The absence of measurable fluorescence when S_1 is $n\pi^*$ is attributed to efficient $^1(n\pi^*)-^3(\pi\pi^*)$ intersystem crossing which, as noted by El-Sayed, is a direct consequence of the strong spin−orbit coupling that exits between singlet and triplet states of different orbital configurations.[16] A solvent-induced inversion of state order such that S_1 becomes $\pi\pi^*$ is believed to occur in those situations where fluorescence is observed. The inversion of $n\pi^*$ and $\pi\pi^*$ states when $n\pi^*$ lies lower in energy in nonpolar solvents is due to the well-known shift to higher energy experienced by $n\pi^*$ states and the shift to lower energy experienced by $\pi\pi^*$ states on going from nonpolar to polar solvents. Hydrogen bonding solvents generally cause the largest blue shift for $n\pi^*$ transitions and the magnitude of the shift has been correlated with the hydrogen bonding strength of the solvent.[17−19] As the INDO/S calculations indicate, and has been found for short polyene ketones and aldehydes where $n\pi^*$ is lower in energy than $\pi\pi^*$, the energy of the $n\pi^*$ state decreases less rapidly than that of the $\pi\pi^*$ state as the number of conjugated double bonds increases.[20,21] Thus, in environments where S_1 is $n\pi^*$ for **1**, **2**, and **3**, the $S_1(n\pi^*)-S_2(\pi\pi^*)$ energy gap is expected to decrease in going from **1** to **3**. The gas-phase INDO/S results show calculated $S_1(n\pi^*)-S_2(\pi\pi^*)$ energy gaps of 8400, 4100, and 3300 cm^{-1} for **1**, **2**, and **3**, respectively.

Figures 7 and 8 present the normalized room-temperature fluorescence, fluorescence excitation, and absorption spectra of **2** and **3** in the alcohol series 1-octanol, 1-butanol, 1-propanol, ethanol, methanol, 2,2,2,-trifluoroethanol (TFE), and hexafluoro-2-propanol (HFIP). Features to note are that the fluorescence spectra red shift to a greater extent than do the absorption spectra as the solvent pK_a decreases. The excitation spectra and absorption spectra for **2** do not overlap completely; whereas there is reasonably good overlap of excitation and absorption spectra for **3** in the series of alcohols. Changing the monitoring wavelength throughout the fluorescence spectra of **2** and **3** does not alter the appearance of the excitation spectra. Specifically, it is found that the excitation spectra of **2** in alcohols are red shifted relative to the absorption spectra, resulting in an apparent dependence of ϕ_f on the S_1 excitation wavelength (for example,

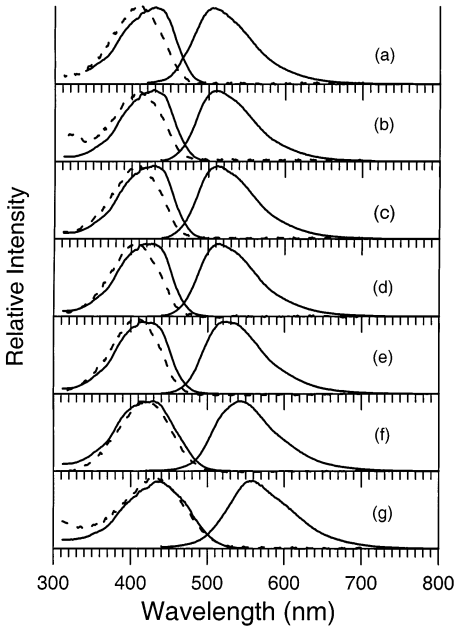

Figure 7. Normalized absorption (dashed line), excitation (left), and fluorescence (right) spectra of **2** in alcohols: (a) 1-octanol; (b) 1-butanol; (c) 1-propanol; (d) ethanol; (e) methanol; (f) TFE; and (g) HFIP. Excitation spectra were obtained by monitoring λ_{max} of the fluorescence.

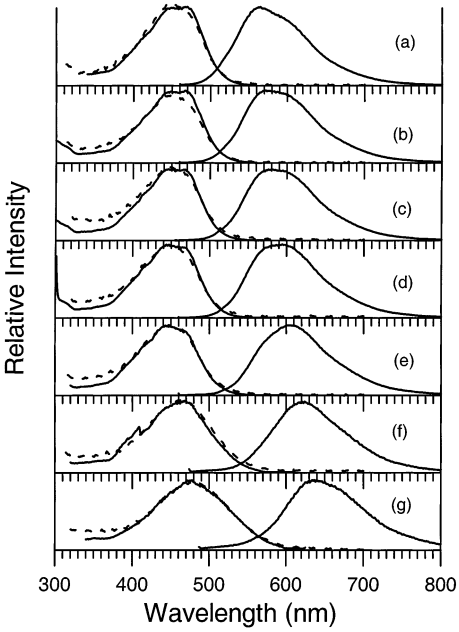

Figure 8. Normalized absorption (dashed line), excitation (left), and fluorescence (right) spectra of **3** in alcohols: (a) 1-octanol; (b) 1-butanol; (c) 1-propanol; (d) ethanol; (e) methanol; (f) TFE; and (g) HFIP. Excitation spectra were obtained by monitoring λ_{max} of the fluorescence.

see Figure 9). The effect is far less pronounced for **2** in the strongly hydrogen bonding solvents TFE and HFIP. The results for **2** in alcohols are strongly reminiscent of the 77 K results reported by Becker[22] for certain polyene ketones and aldehydes, including retinals, in ether/isopentane/ethanol (EPA) and by Christensen and co-workers for 2,4,6,8-decatetraenal in methanol/ethanol at 10 K.[19] The explanation provided in these previous studies is applicable to the results presented here. Within the alcohol solution a mixture of hydrogen bonded and non-hydrogen bonded molecules of **2** exists. For the non-hydrogen bonded members, $n\pi^*$ remains below $\pi\pi^*$ and does not

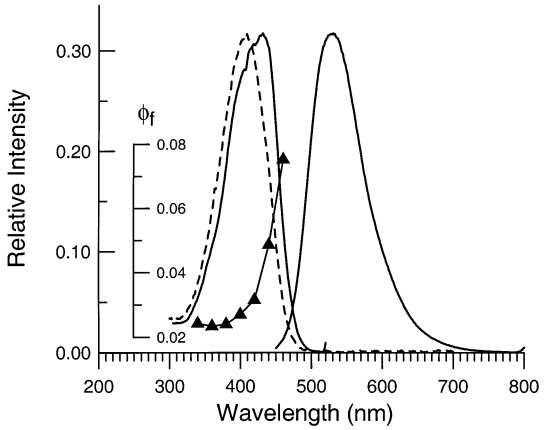

Figure 9. Absorption (dashed line), excitation (left), and fluorescence (right) spectra and fluorescence quantum yield as a function of excitation wavelength for **2** in methanol.

fluoresce. Hydrogen bonding inverts the order of these states and induces fluorescence from S_1 ($\pi\pi^*$). The energy of the $\pi\pi^*$ state of the hydrogen bonded (fluorescing) fraction of molecules undergoes a characteristic red shift relative to that of the non-hydrogen bonded (nonfluorescing) fraction; hence the lack of agreement between the absorption spectrum and the excitation spectrum. Presumably the failure of the nonfluoronated alcohols to completely hydrogen bond with **2** is because much of the solvent is tied up in self-association.[19,23] As with 2,4,6,8-decatetraenal, the extent of complex formation for **2** with the stronger hydrogen-bonding solvents TFE and HFIP appears to be complete as witnessed by the good agreement between excitation and absorption spectra.[19] Unlike decatetraenal, however, a strong enhancement in fluorescence intensity is not observed for **2** in TFE when the temperature is lowered from 100 to 10 K.

Contrary to the situation for **2**, it is found that there is generally good agreement between the excitation and absorption spectra of **3** in alcohols. The conclusion here is that although there is a distribution of hydrogen bonded and nonhydrogen bonded molecules of **3**, the nonhydrogen bonded molecules find themselves in a polar solvent environment that is sufficient to invert $n\pi^*$ and $\pi\pi^*$ and induce fluorescence. The observation of fluorescence from **3** in aprotic polar solvents such as acetonitrile shows that it is possible to achieve state inversion in **3** without forming a hydrogen bonded complex with the solvent.

Because **3** was found to fluoresce in a number of aprotic solvents as well as protic solvents, a more complete study of solvent effects on absorption and fluorescence spectra was carried out. Results for **3** in protic and aprotic solvents are plotted separately in Figure 10. Although not in a perfectly linear manner, it is found that the absorption and fluorescence band maxima shift to lower energy; whereas their difference, the Stokes shift, moves to higher energy when plotted against Δf, the solvent's orientation polarization. The orientation polarization is defined as $\Delta f = (\epsilon - 1)/(2\epsilon + 1) - (n^2 - 1)/(2n^2 + 1)$ where ϵ is the dielectric constant and n is the index of refraction for the solvent. The positive slope for the Stokes shift vs Δf plot is evidence that the dipole moment is larger for **3** in the excited state than in the ground state.[11] It is possible to calculate the dipole moment of **3** in S_1 from the solvent-induced shifts in the absorption and fluorescence spectra by means of the ratio method given in eq 1[24]

$$\mu_e = \mu_g \Delta E_f / \Delta E_a \qquad (1)$$

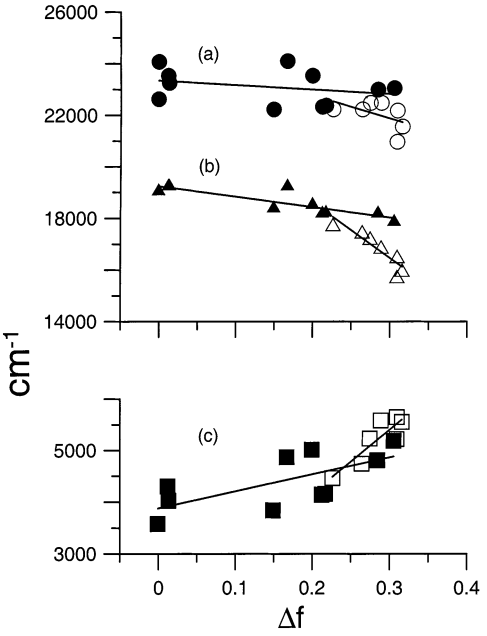

Figure 10. Plot of (a) absorption frequency; (b) fluorescence frequency; (c) Stokes shift against solvent orientation polarization. Open symbols represent protic solvents; solid symbols are for aprotic solvents.

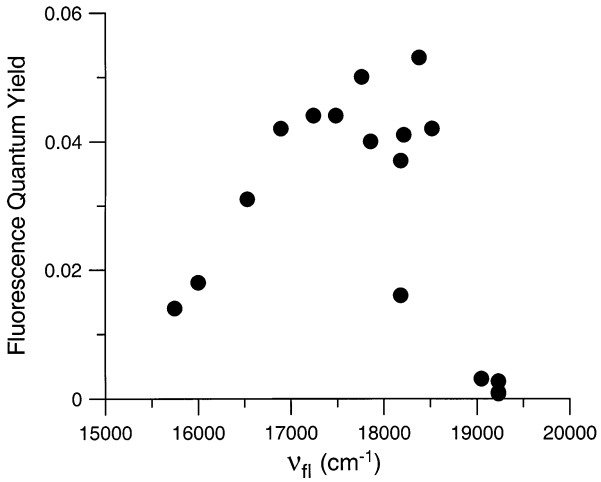

Figure 11. Fluorescence quantum yield of **3** plotted against the frequency of fluorescence in different solvents.

where μ_e and μ_g are the excited state and ground-state dipole moments and ΔE_f and ΔE_g are the solvatochromic shifts for fluorescence and absorption. The major advantage of using this method over the Lippert−Mataga method[25] is that it is not necessary to assume a cavity radius for the solute. In employing eq 1 to determine μ_e the underlying assumptions are that μ_e and μ_g are collinear and that the cavity radius is about the same in both states. Using the PM3 computed value for μ_g (2.79 D), μ_e is calculated to be 6.4 D from the aprotic solvent data and 6.6 D from the protic solvent data. The gas phase INDO/S calculation gives a slightly higher dipole moment of 7.2 D for **3** in the B_2 state.

Fluorescence quantum yields have also been measured for **3** in different solvents and are plotted against the fluorescence frequency maximum for each solvent in Figure 11. It is observed that the quantum yield is approximately 10^{-3} when the fluorescence maximum occurs above 19 000 cm^{-1} (nonpolar solvents), increases sharply to 0.04 ± 0.01 between 19 000 and 17 000 cm^{-1} (polar solvents), and decreases gradually (0.03−0.01) below 17 000 cm^{-1} (alcohols). The radiative rate constants

TABLE 3: Absorption, Excitation, and Fluorescence Spectral Data and Fluorescence Quantum Yields for 2 in Alcohols

solvent	abs. λ_{max} (nm)	exc. λ_{max} (nm)	flu. λ_{max} (nm)	abs. ν_{max} (cm^{-1})	exc. ν_{max} (cm^{-1})	flu. ν_{max} (cm^{-1})	pK_a	ϕ_f	$\lambda_{excitation}$ for ϕ_f (nm)
1-octanol	412	431	505	24 272	23 202	19 802		0.020	409
1-butanol	412	428	510	24 272	23 364	19 608		0.018	409
1-propanol	409	430	512	24 450	23 256	19 531	16.2	0.020	409
ethanol	410	420	515	24 390	23 810	19 417	15.9	0.027	405
methanol	408	416	522	24 510	24 038	19 517	15.5	0.026	400
TFE	420	430	542	23 810	23 256	18 450	12.4	0.035	409
HFIP	432	434	558	23 148	23 041	17 921	9.3	0.013	409

TABLE 4: Absorption and Fluorescence Spectral Data and Fluorescence Quantum Yields for 3

solvent	abs. λ_{max} (nm)	flu. λ_{max} (nm)	abs. ν_{max} (cm^{-1})	flu. ν_{max} (cm^{-1})	Stokes shift (cm^{-1})	Δf	ϕ_f	$\lambda_{excitation}$ for ϕ_f (nm)
carbon disulfide	442	525	22 624	19 048	3577	0.0007	0.0031	400
cyclohexane	415		24 067			0.0002		
carbon tetrachloride	425	520	23 529	19 231	4299	0.0119	0.0008	400
toluene	430	520	23 256	19 231	4025	0.0131	0.0027	400
chloroform	450	544	22 222	18 382	3840	0.1491	0.053	400
ethyl ether	415	520	24 096	19 231	4866	0.1669	0.001	400
ethyl acetate	425	540	23 529	18 519	5011	0.1996	0.042	400
pyridine	448	550	22 321	18 182	4140	0.2124	0.037	400
dichloromethane	447	549	22 371	18 215	4156	0.2171	0.041	410
1-octanol	450	563	22 222	17 762	4460	0.2263	0.050	400
1-butanol	450	572	22 222	17 483	4740	0.2642	0.044	400
1-propanol	445	580	22 472	17 241	5231	0.2746	0.044	410
acetone	435	550	22 989	18 182	4807	0.2843	0.016	415
ethanol	445	592	22 472	16 892	5580	0.2887	0.042	400
acetonitrile	434	560	23 041	17 857	5184	0.3054	0.040	400
HFIP	477	635	20 964	15 748	5216	0.3092	0.014	410
methanol	451	605	22 173	16 529	5644	0.3093	0.031	400
TFE	464	625	21 552	16 000	5552	0.3159	0.018	405

k_f can be determined from a knowledge of ϕ_f and the measured fluorescence lifetime τ, according to $k_f = \phi_f/\tau$. The rate of nonradiative decay from S_1 can be calculated from

$$k_{nr} = (1/\phi_f - 1)k_f \qquad (2)$$

In the absence of experimental values for τ, it is necessary to rely on the method of Strickler and Berg[26] to estimate k_f from the integrated absorption spectra. The radiative rates of decay for **3** in CCl_4 and methanol are calculated by the Strickler and Berg method to be 5×10^8 and 4×10^8 s^{-1}, respectively. From these values of k_f and the measured ϕ_f, the k_{nr} values are calculated from eq 2 to be 6×10^{11} (CCl_4) and 1×10^{10} s^{-1} (methanol) for **3**. Limited as they may be,[27] the data obtained in these two solvents suggest that the order of magnitude decrease in ϕ_f for **3** in solvents where emission occurs above 19 000 cm^{-1} compared to its value in those solvents where the fluorescence occurs at lower frequencies is due primarily to a larger value for k_{nr}. This is contrary to the trend expected from the energy gap law for internal conversion which predicts that the rate of internal conversion should increase as the energy gap between S_1 and S_0 decreases.[28] Explanations for the enhanced rate of nonradiative decay for **3** in solvents where emission occurs at frequencies above 19 000 cm^{-1} can be found by considering that it is in these nonpolar solvents (CS_2, CCl_4, toluene) that **3** is expected to have the smallest $S_1(\pi\pi^*)-S_2(n\pi^*)$ energy gap. There are two pathways by which this small energy gap could result in efficient nonradiative decay of S_1. One is through an enhancement in the rate of intersystem crossing and the other is through an enhancement of the rate of internal conversion. If $^3n\pi^*$ lies between $S_1(\pi\pi^*)$ and $T_1(\pi\pi^*)$, efficient intersystem crossing could account for the weak fluorescence. Because of the dramatic difference in oscillator strengths, k_f for $S_1(\pi\pi^*)$ is expected to be much larger than that for $S_1(n\pi^*)$. Hence, a small amount of fluorescence can be observed for **3** in these solvents compared to alkane solvents where no fluorescence has been observed and where S_1 is $n\pi^*$. A blue shift of the $^3n\pi^*$ state in polar or hydrogen bonding solvents could shift it above $S_1(\pi\pi^*)$ and cut off this path for intersystem crossing. An alternative mechanism for solvent-dependent intersystem crossing that does not require $^3n\pi^*$ to be located below $S_1(\pi\pi^*)$ is second-order vibronic spin−orbit coupling.[29] Here, increasing the $n\pi^*-\pi\pi^*$ energy gap with solvent diminishes the degree of state mixing which in turn reduces the rate of intersystem crossing.

The enhanced internal conversion pathway involves the "proximity effect" where vibronic interaction between closely spaced $n\pi^*$ and $\pi\pi^*$ states is expected to lead to the distortion and displacement of the potential energy surfaces of the coupled states. Lim has argued through theory and experiment that such distortion/displacement of S_1 can dramatically increase the rate of internal conversion.[30] Any influence (solvent, substituents) that increases the $n\pi^*-\pi\pi^*$ energy gap between strongly coupled states would reduce the vibronic coupling between them and the associated distortion/displacement of potential energy surfaces, thus decreasing the rate of internal conversion. For many nitrogen heterocylic and aromatic carbonyl compounds that do not fluoresce or fluoresce weakly in nonpolar aprotic solvents, it has been observed that a switch to protic solvents greatly increases ϕ_f. Studies indicate that for some of these molecules the change in fluorescence behavior cannot be attributed to a change in singlet−triplet intersystem crossing.[31] The extent to which each of these pathways contribute to k_{nr} when S_1 of **3** is above 19 000 cm^{-1} awaits further investigation.

The rate that ϕ_f drops off with decreasing energy when S_1 of **3** is below 17 000 cm^{-1} appears to be consistent with the energy gap law for internal conversion which predicts an exponential dependence of k_{ic} on ΔE, the S_1-S_0 energy gap[20]

$$k_{ic} = Ce^{-\alpha\Delta E} \qquad (3)$$

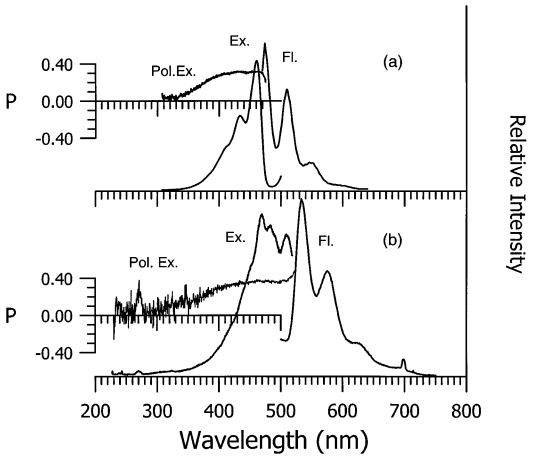

Figure 12. (a) Fluorescence, fluorescence excitation, and polarized excitation spectra of **2** in ethanol/methanol (4:1) glass at 77 K. (b) Fluorescence, fluorescence excitation, and polarized excitation spectra of **3** in ethanol/methanol (4:1) glass at 77 K.

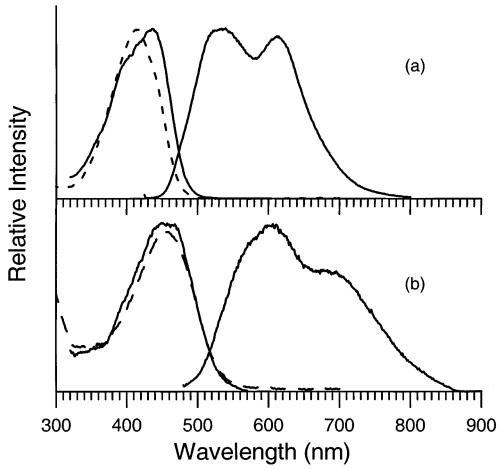

Figure 13. (a) Absorption (dashed line), excitation (left), and fluorescence (right) spectra of **2** in acetic acid. (b) Absorption (dashed line), excitation (left), and fluorescence (right) spectra of **3** in acetic acid.

The room-temperature fluorescence properties of **2** and **3** are summarized in Tables 3 and 4.

Fluorescence, fluorescence excitation, and polarized excitation spectra were measured for **2** and **3** at 77 K in an ethanol/methanol (4:1) glass and are shown in Figure 12. In comparing the room-temperature spectra of **2** and **3** in ethanol with the 77 K spectra in ethanol/methanol, it is observed that the spectra change from broad featureless bands to spectra exhibiting well-resolved vibronic structure. It is also seen that the low temperature absorption spectra are red shifted and the fluorescence spectra blue shifted relative to the room temperature spectra, resulting in a much smaller Stokes shift. Small Stokes shifts are commonly observed for molecules in low temperature glasses and are attributed to the inability of the solvent matrix to reorient and stabilize the molecule during the excited state lifetime. The red shift of the absorption spectrum in going from a room temperature liquid to a low temperature glass for a polar molecule in a polar solvent is also frequently observed and may be related to the thermochromic shift discussed by Suppan.[32] The decrease in the degree of positive polarization observed toward the short wavelength tail of the strong $B_2(y) \leftarrow A_1$ transition for **2** and **3** may be due to the presence of a weak underlying transition of perpendicular polarization. As noted earlier, the INDO/S calculations do predict a weak $A_1(z) \leftarrow A_1$ transition (S_3) to occur in this region.

Excited-State Proton Transfer. The room-temperature absorption, fluorescence, and fluorescence excitation spectra of **2** and **3** in acetic acid are presented in Figure 13. Fluorescence is not observed for **1** in acetic acid. It is seen that the fluorescence spectra of both **2** and **3** consist of two overlapping bands (535, 615 nm for **2**; 604, 685 nm for **3**). The excitation spectrum of each compound does not change when the monitoring wavelength is moved from the shorter wavelength fluorescence band to the longer wavelength band. However, it is observed that the longer wavelength fluorescence band decreases in relative intensity and eventually disappears when the acid solution is diluted gradually with water (pH increased). This, along with additional evidence that will be presented in a subsequent publication that deals with ground and excited-state properties of the protonated cations of **1**, **2**, and **3**, leads us to assign the longer wavelength fluorescence band to emission from protonated **2** and **3**. The protonated cations are formed on the excited-state surface and emit before returning to the ground state.[33] The shorter wavelength band corresponds to emission from the hydrogen bonded (unprotonated) ketone. A transfer of electron charge density to the carbonyl oxygen atom upon excitation from S_0 to $S_1(\pi\pi^*)$ makes **2** and **3** stronger bases in the excited state, thus promoting excited-state proton transfer from acetic acid. A reduction in electron charge density on the oxygen atom occurs when S_1 is $n\pi^*$ as appears to be the case for **1** in acetic acid, making the molecule a weaker base in S_1. It is possible to protonate S_0 of **1**, **2**, and **3** using strongly acidic media.[34]

References and Notes

(1) (a) Barnabus, M. V.; Liu, A.; Trifunac, A. D.; Krongauz, V. V.; Chang, C. T. *J. Phys. Chem.* **1992**, *96*, 212. (b) Chambers, W. J.; Eaton, D. F. *J. Imaging Sci.* **1986**, *30*, 230. (c) Baum, M. D.; Henry, C. P. U.S. Patent 3,652,275.

(2) (a) Pivovarenko, V. G.; Klueva, A. V.; Doroshenko, A. O.; Demchenko, A. P. *Chem. Phys. Lett*. **2000**, *325*, 389. (b) Das, P. K.; Pramanik, R.; Banerjee D.; Bagchi, S. *Spectrochim. Acta A* **2000**, *56*, 2763.

(3) Doroshenko, A. O.; Grigorovich, A. V.; Posokhov, E. A.; Pivovarenko, V. G.; Demchenko, A. P. *Mol. Eng.* **1999**, *8*, 199.

(4) (a) Kawamata, J.; Inoue, K.; Inabe, T. *Bull. Chem. Soc. Jpn.* **1998**, *71*, 2777. (b) Kawamata, J.; Inoue, K.; Inabe, T.; Kiguchi, M.; Kato, M.; Taniguchi, Y. *Chem. Phys. Lett.* **1996**, *249*, 29. (b) Kaatz, P.; Shelton, D. P. *J. Chem. Phys.* **1996**, *105*, 3918. (c) Kawamata, J.; Inoue, K.; Inabe, T. *Appl. Phys. Lett.* **1995**, *66*, 3102.

(5) (a) Theocharis, C. R.; Alison, M. C.; Hopkin, S. E.; Jones, P.; Perryman, A. C.; Usanga, F. *Mol. Cryst. Liq. Cryst.* **1998**, *156*, 85. (b) Frey, H.; Behmann, G.; Kaupp, G. *Chem. Ber.* **1987**, *120*, 387. (c) Theocharis, C. R.; Jones, W.; Thomas, J. M.; Montevalli, M.; Hursthouse, B. *J. Chem. Soc., Perkin Trans. 2* **1984**, 71. (d) Theocharis, C. R.; Thomas, J. M.; Jones, W. *Mol. Cryst. Liq. Cryst.* **1983**, *93*, 53.

(6) (a) Issa, R. M.; Etaiw, S. H.; Issa, I. M.; El-Shafie, A. K. *Acta Chim. Acad. Sci. Hung., Tomus* **1976**, *89*, 381. (b) Farrel, P. G.; Read, B. A. *Can. J. Chem.* **1968**, *46*, 3685.

(7) (a) Hudson, B. S.; Kohler, B. E.; Shulten, K. In *Excited States*; Lim, E. C., Ed.; Academic Press: New York, 1982; Vol. 6, pp 1−95. (b) Christensen, R. L. In *Advances in Phtosynthesis: The Photochemistry of Carotenoids*; Frank, H. A., Young, A. J., Britton, G., Cogdell, R. J., Eds.; Kluwer Academic Publishers: Dordrecht, The Netherlands, 1999; Vol. 8, pp 137−159.

(8) Iranpoor, N.; Kazemi, F. *Tetrahedron* **1998**, *54*, 9475.

(9) Maeta, H.; Suzuki, K. *Tetrahedron Lett.* **1993**, *34*, 341.

(10) Rechthaler, K.; Köhler *Chem. Phys. Lett.* **1994**, *189*, 99.

(11) Lakowicz, J. R. *Principles of Fluorescence Spectroscopy*, 2nd ed.; Kluwer Academic/Plenum Publishers: New York, 1999.

(12) Stewart, J. J. P. *J. Comput. Chem*. **1989**, *1*, 209.

(13) Ridley, J.; Zerner, M. *Theor. Chim. Acta* **1973**, *32*, 111.

(14) Sanford, E. M.; Paulisse, K. W.; Reeves, J. T. *J. Appl. Polym. Sci*. **1999**, *74*, 2255.

(15) Baltrop, J.; Coyle, J. D. *Principles of Photochemistry*; Wiley & Sons: New York, 1978; p 62.

(16) El-Sayed, M. A. *J. Chem. Phys.* **1963**, *38*, 2834.

(17) Jaffé, H. H.; Orchin, M. *Theory and Applications of Ultraviolet Spectroscopy*; John Wiley & Sons: New York, 1962; p 186.
(18) Brealey, G. J.; Kasha, M. *J. Am. Chem. Soc*. **1955**, *77*, 4462.
(19) Papanikolas, J.; Walker, G. C.; Shamamian, V. A.; Christensen, R. L.; Baum, J. C. *J. Am. Chem. Soc*. **1990**, *112*, 1912.
(20) Klessinger, M.; Michl, J. *Excited States and Photochemistry of Organic Molecules*; VCH Publishers: New York, 1995.
(21) Das, P. K.; Becker, R. S. *J. Phys. Chem*. **1978**, *82*, 2081.
(22) (a) Das, P. K.; Becker, R. S. *J. Phys. Chem*. **1978**, *82*, 2093. (b) Takemura, T.; Das, P. K.; Hug, G.; Becker, R. S. *J. Am. Chem. Soc*. **1978**, *100*, 2626. (c) Takemura, T.; Das, P. K.; Hug, G.; Becker, R. S. *J. Am. Chem. Soc*. **1976**, *98*, 7099.
(23) (a) Fletcher, A. N. *J. Phys. Chem.* **1972**, *76*, 2562. (b) Kuhn, L. P. *J. Am. Chem. Soc.* **1952**, *74*, 2492.
(24) Suppan, P. *Chem. Phys. Lett.* **1983**, *94*, 272.
(25) (a) Lippert, E. *Z. Electrochem.* **1957**, *61*, 962. (b) Mataga, N.; Kaifu, Y.; Koizumi, M. *Bull. Chem. Soc. Jpn.* **1956**, *29*, 465.
(26) Strickler, S. J.; Berg, R. A. *J. Chem. Phys.* **1962**, *37*, 814.
(27) A limited supply of **3** prevented us from obtaining the extinction coefficients in a wide variety of solvents.
(28) Siebrand, W. *J. Chem. Phys.* **1967**, *46*, 440/2411.
(29) (a) Lim, E. C.; Yu, J. M. H. *J. Chem. Phys.* **1967**, *47*, 3270. (b) Lim, E. C.; Yu, J. M. H. *J. Chem. Phys.* **1966**, *45*, 4742.
(30) Lim, E. C. *J. Phys. Chem.* **1986**, *90*, 6770.
(31) Madej, S. L.; Okajima, S.; Lim, E. C. *J. Chem. Phys*. **1976**, *65*, 1219.
(32) Suppan, P. *Photochem. Photobiol., A* **1990**, *50*, 293.
(33) Moomaw, W. R.; Anton, M. F. *J. Phys. Chem*. **1976**, *80*, 2243.
(34) Connors, R. E.; Ucak-Astarlioglu, M. G. Unpublished results.